ACS APPLIED MATERIALS & INTERFACES

Letter

www.acsami.org

# ALD Zn(O,S) Thin Films' Interfacial Chemical and Structural Configuration Probed by XAS

Anup L. Dadlani,[†] Shinjita Acharya,[‡] Orlando Trejo,[‡] Fritz B. Prinz,[‡,§] and Jan Torgersen*[,‡]

[†]Department of Chemistry, [‡]Department of Mechanical Engineering, and [§]Department of Materials Science and Engineering, Stanford University, Stanford, California 94305, United States

Supporting Information

**ABSTRACT:** The ability to precisely control interfaces of atomic layer deposited (ALD) zinc oxysulfide (Zn(O,S)) buffer layers to other layers allows precise tuning of solar cell performance. The O K- and S K-edge X-ray absorption near edge structure (XANES) of ~2−4 nm thin Zn(O,S) films reveals the chemical and structural influences of their interface with ZnO, a common electrode material and diffusion barrier in solar cells. We observe that sulfate formation at oxide/sulfide interfaces is independent of film composition, a result of sulfur diffusion toward interfaces. Leveraging sulfur's diffusivity, we propose an alternative ALD process in which the zinc precursor pulse is bypassed during $H_2S$ exposure. Such a process yields similar results to the nanolaminate deposition method and highlights mechanistic differences between ALD sulfides and oxides. By identifying chemical species and structural evolution at sulfide/oxide interfaces, this work provides insights into increasing thin film solar cell efficiencies.

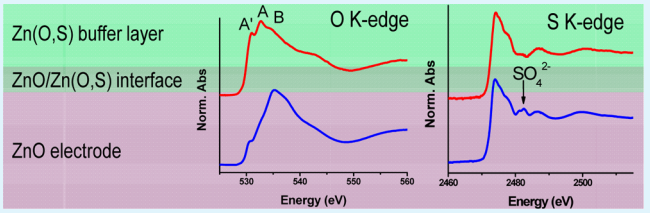


**KEYWORDS:** *X-ray absorption near edge structure (XANES), Zn(O,S), atomic layer deposition (ALD), ternary oxide films, electronic structure*

Atomic layer deposited (ALD) zinc oxysulfide (Zn(O,S)) films have garnered increasing attention as promising buffer layers in solar cells stemming from the ease with which their composition and thickness can be tuned, a flexibility that allows for adjusting the films' band gap, conduction band offset and conductivity, among many other properties.[1−3] The versatility of Zn(O,S) to be paired up with several absorber layers (SnS, CIGS, CIS, CZTS) and its large bandgap range ($E_g$ ≈ 2.6−3.8 eV)[4] may allow it to replace the more commonplace but highly toxic CdS buffer layers.

Adjusting sulfur content to obtain a slightly positive conduction band offset (CBO ≤ 0.5 eV)[5] and decreasing buffer layer thickness[6,7] reduces interfacial and bulk carrier recombination and allows for straightforward optimization of cell performance.[8−10] However, to date, there is still controversy on the degree of Zn(O,S) bandgap bowing with sulfur content and thickness.[5,10,11] This is largely due to the rapid diffusion of sulfur inside the buffer layer toward the substrate interface, which complicates band alignment.[7,11] It becomes particularly problematic in metal-sulfide ALD, where low growth rates necessitate the films' long exposure to elevated temperatures, favoring reconfiguration.[12] As a result, Zn(O,S) buffer layers perform differently depending on deposition technique[13] and strategy.[5]

X-ray absorption near edge structure (XANES) is capable of revealing oxidation states, coordination chemistry, molecular orbitals, band structure, local displacement and chemical short-range order information[14] and has been established as a powerful technique for studying interfaces,[15] compositional effects,[9] and electronic structure[16] in ALD films. Through XANES, we recently discovered[9] the electronic−geometric structure relationship behind the band gap bowing. Infiltration of sulfur into ZnO gives rise to S 3p−Zn 4sp−O 2p hybridized orbitals in the conduction band as seen in both O and S K-edges, where electron donating behavior of sulfur[17] affects the ionicities and bond lengths of the system. However, in that reference work, Zn(O,S) films were deposited on $TiO_2$ nanoparticles (NPs), a relevant electrode for dye sensitized solar cells, but not used in CIGS based devices.[18] In CIGS architectures, the buffer has interfaces with two films: (1) the top electrode, typically an n-type intrinsic or Al-doped ZnO and (2) a p-type CIGS absorber layer.[19] To prevent sulfur diffusion and the formation of an interfacial current blocking ZnS film,[7,20] the CIGS is often coated with a thin layer of ZnO before the deposition of Zn(O,S).[5] Hence, in a common CIGS device, Zn(O,S) interfaces with ZnO on both sides. Knowledge on the electronic structure of a ZnO/Zn(O,S) interface is therefore indispensable. In what follows, we will explore the O K- and S K-edges of ~2−4 nm thin Zn(O,S), elaborating on electronic structure differences to thick films, substrate, and composition dependencies. We will show how sulfides behave differently from oxides and may evolve in a completely different manner than is commonly understood.

**Received:** April 5, 2016
**Accepted:** May 25, 2016
**Published:** May 25, 2016

  

DOI: 10.1021/acsami.6b04000
*ACS Appl. Mater. Interfaces* 2016, 8, 14323−14327

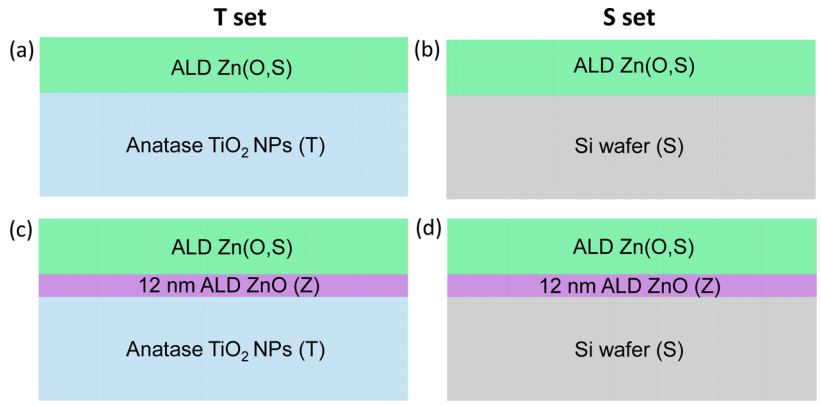


**Figure 1.** Schematics of the sample architectures. The sample architectures for the T (a, c) and S (b, d), sample sets are shown. For both sets, 10%, 20%, and 33% $H_2S/(H_2S+H_2O)$ pulse ratios were employed for ALD Zn(O,S) thick (~50−60 nm) and thin films (~2−4 nm). (The thickness of these samples may not be accurate due to the ineffectiveness of characterization at this regime.) We assumed the same ALD growth rate as reported past the film's nucleation phase. (a) ALD buffer layers were deposited on nanoporous $TiO_2$ substrates (T). (b) ALD buffer layers were deposited on planar Si substrates (S). (c) 12 nm ALD ZnO (Z) introduced between anatase $TiO_2$ NPs and buffer layer, labeled (TZ). (d) 12 nm ALD ZnO (Z) introduced between Si substrate and buffer layer, labeled (SZ).

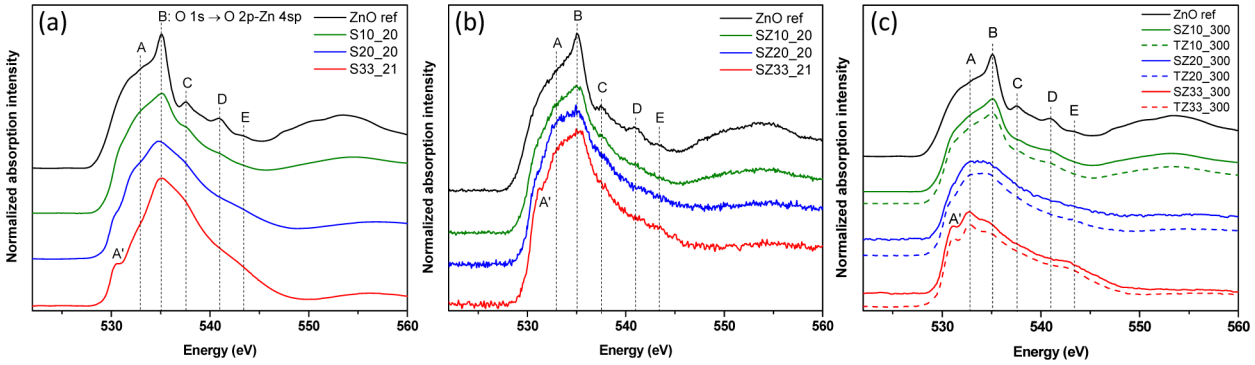


**Figure 2.** (a) O K-edge TEY spectra of 20 cycles Zn(O,S) with 10% (green), 20% (blue), and 33% (red) $H_2S/(H_2S+H_2O)$ cycle ratios grown on Si substrate. The 60 nm ALD ZnO reference (black) deposited on Si substrate has five main features that appear, labeled A−E corresponding to O 1s electronic excitation to O 2p−Zn 4sp unoccupied states in the conduction band. O K-edge AEY spectra are shown in Figure S4. All spectra were background subtracted and atomically normalized in the energy region from 548 to 560 eV. O K-edge spectra of (b) thin samples deposited on Si coated with 12 nm of ALD ZnO (AEY) and (c) ~50−60 nm Zn(O,S) films deposited on ZnO-coated Si (solid) and $TiO_2$ NPs (dashed), both TEY. As a reference sample, we show the O K-edge of 60 nm ALD ZnO in both panels.

Figure 1 shows the sample architectures that were investigated in this work. The sample labels will follow the nomenclature; Lettersnumber_cycles, where letters indicate substrate (T for $TiO_2$ NPs, S for $SiO_2$, TZ for 12 nm ZnO coated $TiO_2$ NPs and SZ for 12 nm ZnO coated Si substrates), number gives $H_2S/(H_2S+H_2O)$ cycles ratio (33%, 20% and 10%) and cycles denotes the total number of ALD cycles. Experimental details of the samples are provided in Supporting Information and are in agreement with previous reports.[3,21,13]

The O K-edge XANES total electron yield (TEY) spectra of thin samples (20 cycles) deposited on anatase $TiO_2$ NPs (Figure 1a) are shown in Figure S2 (information obtained from TEY spectra is from a few nm below the top surface). The overwhelming signal from the $TiO_2$ substrate did not allow for a direct comparison of thin Zn(O,S) films to our previous work,[9] because the thin films almost look identical to the $TiO_2$ reference (Figure S2). When growing thin Zn(O,S) films on flat $SiO_2$ substrates (Figure 1b), clear thin film and interface information is obtained from the O K-edge TEY XANES spectra (Figure 2a). The features A−E correspond to the electronic excitation from O 1s states to unoccupied states in the conduction band of ZnO, which is made up of O 2p−Zn 4sp states.[22] Sample S10_20 bears closest resemblance to the reference sample. Its features are broadened, D − E are lost and the B/A ratio is less. In sample S20_20, feature C disappears and feature A′ weakly appears indicating the hybridization from S 3p orbitals.[9] A′ is most prominent in sample S33_21.

Similar to the thick films grown on Si (Figure S3), the longer range order (peaks C, D, and E) of the thin films has not fully developed. Auger electron yield (AEY) spectra, which reveal information from the very top surface of the sample (Figure S4), appear similar, suggesting that Figure 2a already contains information on the $Zn(O,S)/SiO_2$ interface. The energy onset of all the thin film spectra are slightly shifted to higher energies in comparison to the thick films (Figure S5). This likely indicates an increase in the band gap.[9] The spectral weight of 20 and 33% films shifts to higher energy. This results in a differently appearing peak A in the thin film regime. It is weak in the 20% case and disappears in the 33% sample. Due to this shift, feature A′ also appears differently. These changes in the electronic structure might explain the differences in thin film device performance with thickness despite fabricating samples in the same way.[6,7]

In solar cell devices, the ZnO/Zn(O,S) is a relevant interface to investigate and one that has not been carefully considered thus far.[5] To obtain information on Zn(O,S)/ZnO interfaces,


DOI: 10.1021/acsami.6b04000
ACS Appl. Mater. Interfaces 2016, 8, 14323−14327

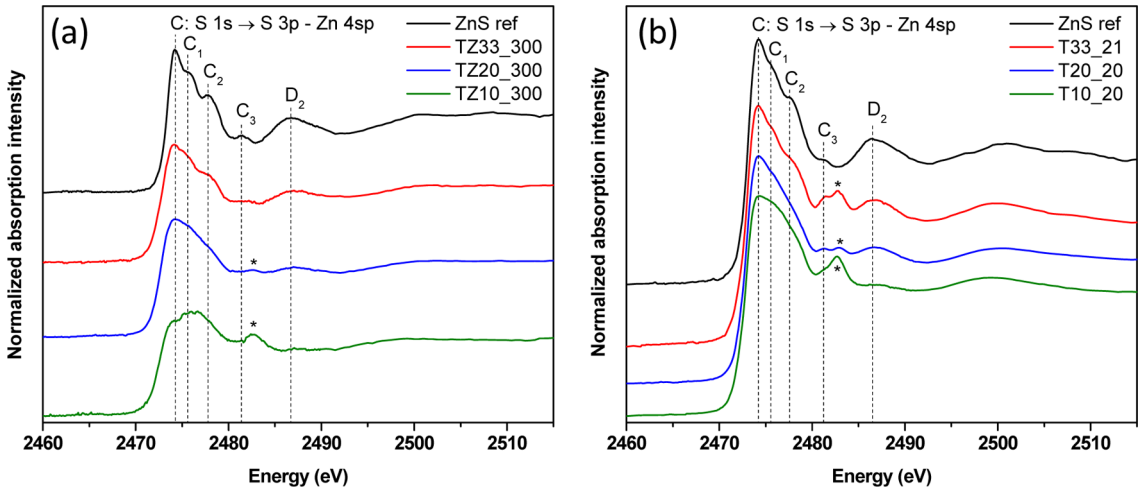


**Figure 3.** (a) S K-edge XANES total fluorescence yield (TFY) spectra of thick samples deposited on anatase $TiO_2$ NPs substrate (T) with 12 nm of ALD ZnO (Z) deposited in between. (TFY gives information from tens of nm from the top surface). As a reference sample, 34 nm of ALD ZnS (300 cycles) was deposited on anatase $TiO_2$ NPs. The main S K-edge absorption can be analyzed as a transition from S 1s to hybridized states with orbital contributions from S 3p and Zn 4sp. Starred peak pertains to presence of sulfate. (b) S K-edge XANES TFY spectra of thin samples deposited on anatase $TiO_2$ NPs. The reference sample was TZnS_20, (20 cycles ZnS deposited on anatase $TiO_2$ NPs). The presence of the peak at 2482.5 eV (starred) is indicative of sulfate and is there in all the thin samples, regardless of stoichiometry. All spectra were background subtracted and atomically normalized in the energy region from 2500 to 2510 eV.

we coated Si with 12 nm of ZnO before growing Zn(O,S) (Figure 1d). Samples with 10% $H_2S$ cycle ratio appear similar when grown on ZnO (Figure 2b) and Si (Figure 2a). However, regarding both 20 and 33% samples grown on ZnO, feature A′ is less pronounced than on Si. The onset of the 33% sample has a prominent red shift when grown on ZnO (see comparison in Figure S6). This change in the spectrum is significant, because it means that the unoccupied density of states is shifted to lower energies, suggesting that the band gap of the sample is lower.

Comparing thin (∼2−4 nm) with thick (∼50−60 nm) Zn(O,S) films grown on ZnO, we observe the absence of peak A in the thick 10% sample (Figure 2b). Key features of the 20% sample remain similar in thick samples. At this composition, Zn(O,S) seems to grow more homogeneously. This can be due to the highly distorted structure which seems to be minimally influenced by the substrate. The 33% samples appear very different in the two thickness regimes. In thick samples, feature A′ is more distinct and shifted to higher energy. Feature A has developed to higher intensity than feature B, shifting its spectral weight to lower energy. The 10% film develops feature D with thickness. The 20% sample does not develop any high energy features indicating that it is limited in order. We can conclude that samples with high distortion from either crystal structure grow homogeneously with thickness, whereas the substrate distorts samples with compositions close to ZnO or ZnS. These changes in the film morphology with film thickness are likely due to relaxation events and might play a role in the observed performance differences with buffer layer thickness.[7]

In Figure 3a, we investigate the effects of this interface on the electronic structure of ∼50−60 nm (300 cycles) thick Zn(O,S) buffer layers (architecture in Figure 1c) in the S K-edge XANES spectra. As a reference to the Zn(O,S) films, we show an ALD grown 34 nm thick ZnS (300 cycles) on $TiO_2$ NPs, which matches with literature.[23]

The particular sensitivity of S K-edge XANES,[24] allows us to precisely investigate sulfur's bonding environment (Figure 3). Among the many features present, a peak that does not belong to ZnS is present at 2482.5 eV (starred), only barely visible in TZ20_300, but unmistakably pronounced in TZ10_300. The peak at this energy signifies the formation of sulfate species indicating sulfur's presence in +6 oxidation state. This was observed in Zn(O,S) films grown on $TiO_2$ NPs;[9] however, there the formation was far less pronounced. It appears sulfate formation is more favorable at ZnO/Zn(O,S) interfaces than at $TiO_2$/Zn(O,S) interfaces.

Sulfate changes the electronic and chemical structure of ZnO and its interface to the absorber layer. It is detrimental for device performance. It leads to an increase in resistivity and a loss in fill factor, which is commonly observed in old, degraded devices that are continuously exposed to high humidity and heat.[25,26]

ALD growth of ZnO and Zn(O,S) requires long process times at elevated temperature and recurring exposures to evaporated $H_2O$. These conditions seem to favor sulfate formation and might explain the difference in device performance with ALD Zn(O,S) films, which are lower as compared to sputtered or chemical bath deposited films.[13]

Samples with high sulfur concentration (33%) do not contain sulfate. The sulfate may still potentially form at the Zn(O,S)/ZnO interface, but the sulfide signal is probably overwhelming the sulfate in this case.[25] To verify this hypothesis, we have to look at the XANES of ultrathin films comprising mostly interfacial information.

We grew ∼2−4 nm Zn(O,S) films of different sulfur concentrations on $TiO_2$ NPs (Figure 1a) where S K-edge spectra are shown in Figure 3b. As a reference, we show ∼2 nm of ALD ZnS. We were not successful in obtaining spectra of Zn(O,S) films grown on $TiO_2$ NPs coated with thin ZnO layers. The signal-to-noise ratio was too weak to obtain Zn(O,S) spectra in the S K-edge. Sample T33_21 has all the peaks as the reference sample, however, features $C_2$ and $D_2$ are weaker, while $C_3$ is stronger. Sample T20_20 loses features $C_1$ and $C_2$. Sample T10_20 also no longer has features $C_1$ and $C_2$ and features $C_3$ and $D_2$ seem to have nearly disappeared. The loss of features just past the main edge ($C_1$, $C_2$, and $C_3$) are due


DOI: 10.1021/acsami.6b04000
ACS Appl. Mater. Interfaces 2016, 8, 14323−14327

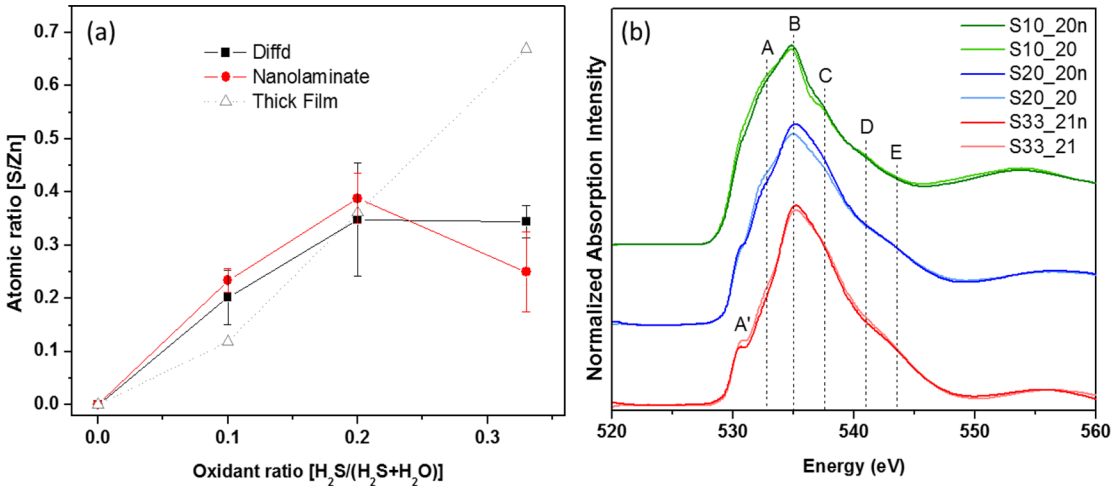


**Figure 4.** (a) S/Zn ratio determined as a function of $H_2S/(H_2S + H_2O)$ oxidant pulses by XPS survey scans (peak integration of Zn $2p_{3/2}$ and S 2p, 20 cycles, Si ⟨100⟩, 160 °C deposition temperature). Deposition of ultrathin samples by the conventional laminar method (red circles), Diffd method (black squares), and thick films by the laminar method (gray triangles). (b) O K-edge XANES TEY of thin film samples in (a), where Diffd method is demarcated by "n".

to distortion of the lattice away from cubic ZnS.[23] With decreasing S concentration, we see feature $C_3$'s intensity gradually decreasing. Interestingly, in the ultrathin film regime, all compositions closely resemble ZnS, whereas in the thick samples, the one with the lowest S content is quite dissimilar (Figure 3a). In the thin film regime, the formation of an interfacial sulfate can now be detected in all films, independent from stoichiometry (starred). The sulfate peak is again most prominent at the lowest S concentration (T10_20), however, T20_20 now has the smallest sulfate peak intensity. Unlike in spectra taken from thick film (TZ33_300, Figure 3a), its thin film counterpart shows sulfate formation (T33_21, in Figure 3b).

When growing thick Zn(O,S) films on $TiO_2$ NPs, sulfate formation seems limited. For 50−60 nm thick films, < 1% sulfate was detected in samples with 10% $H_2S$ cycle ratio.[9] In the ultrathin film regime, however, all samples show sulfate. We hence hypothesize that sulfate evolves at the interface. This seems more likely on ZnO/Zn(O,S) than on $TiO_2$/Zn(O,S) interfaces as more sulfate was present in the thick TZ10_300 (Figure 3a) grown on ZnO. Even TZ20_300 shows a low sulfate peak, whereas it remained absent in a 20% sample grown directly on $TiO_2$ NPs. This is likely due to ZnO's tendency to form $ZnSO_4$ following interdiffusion of S into the ZnO lattice.[25]

Composition wise, thin films are similar to thick films with lower sulfur content (Figure 4a). At 10% $H_2S$ cycle ratio, the S/Zn content is higher in thin films. After 20%, the thin films' S/Zn content seems to plateau. In thick Zn(O,S) films, such a S/Zn compositional independence was reported only at higher $H_2S$ cycles and S/Zn ratios.[11] Generally, Zn(O,S) films with low sulfur content are better buffer layers, however, in thin films, the optimum relative $H_2S$ cycle ratio ($H_2S/(H_2S+H_2O)$) is higher than for thick films.[10,11] Our results explain why thin films with higher $H_2S$ cycle numbers can yield better performances as sulfur incorporation seems to be limited when Zn(O,S) first begins to grow. The drastic electronic structure difference of the thin film 33% sample compared to its thick counterpart also supports this hypothesis.

Sulfur diffusion becomes problematic as it especially blurs interfaces in multilayer sulfide laminate and in metal-oxide/sulfide interfaces. Films like ZnO limit diffusion, but do not entirely prevent it.[12] However, this challenge also presents an opportunity. Leveraging sulfur's diffusivity, we propose a novel Zn(O,S) composite film deposition strategy.

In Figure 4a, we compare the S/Zn compositions of thin Zn(O,S) deposited by the conventional sequential nanolaminate ALD Zn(O,S) process (diethyl zinc (DEZ)−$H_2O$−DEZ−$H_2S$) and a diffusion facilitated film deposition (Diffd) strategy (DEZ−$H_2O$−$H_2S$). To show that diffusion plays a significant role for Zn(O,S) films and for sulfides in general,[12] we employ the Diffd method, in which, according to the general ALD principle,[27] ZnS should not grow by simply exposing the −OH terminated surface to $H_2S$. Yet, when employing Diffd, the compositions of Zn(O,S) films seem to be nearly equivalent to those obtained with the nanolaminate method until a cycle ratio of 20% $H_2S$. At 33%, however, the composition drops with the conventional strategy, where it plateaus when employing Diffd. The compositional changes are not as drastic in comparison with thick samples. To draw definitive conclusions on the compositional differences and trends obtained with either deposition technique, we require studies with higher $H_2S$ cycle numbers, which is beyond the scope of this work.

Here, we focus on the deposition technique dependent electronic structure differences (O K-edge Figure 4b). Employing Diffd, the spectra appear slightly broader with a decreased B/A peak ratio. Due to diffused sulfur's incorporation into the ZnO lattice, the local bonding environment deviates slightly more than in nanolaminate Zn(O,S) films. This influences the orbital mixing in S 3p - Zn 4sp - O 2p and is most pronounced in the 20% sample. The Diffd 33% sample closely resembles the nanolaminate sample showing a slightly more distinct A′ peak. In general, both deposition strategies seem to yield films similar in electronic structure and composition. It is interesting to note that despite having similar S/Zn ratios for the 20 and 33% thin films, the electronic and hence geometric structure of these thin films are different (Figures 3b and 4b), indicating that the incorporation of sulfur is occurring differently.

Regardless of the specific film composition and interface at play, these findings show that metal-sulfide and especially mixed metal-oxide/metal-sulfide ALD require deeper investigations. From the current understanding of the $H_2S$ oxidation step in the nanolaminate protocol, $H_2S$ first dissociates, then


DOI: 10.1021/acsami.6b04000
ACS Appl. Mater. Interfaces 2016, 8, 14323−14327

protonates the ligand and creates a surface thiol on the metal.[27,28] In the context of these findings, we might have to revise this concept. We speculate that only a limited number of DEZ surface sites, available after the first ZnS half cycle, react with $H_2S$, protonate the ligands and leave surface thiols. The dominant mechanism seems to be the diffusion of sulfur deeper into the growing film after $H_2S$ exposure. Reactive surface sites remain available for the next $H_2O$ pulse.

In summary, we carefully investigated substrate, thickness, and precursor sequence effects on the electronic and atomic structure of Zn(O,S) thin films deposited by ALD. We observe several discernible differences in the thin versus thick film regime as revealed by the O and S K-edge XANES spectra, especially for the 33% films. Sulfur deficient (10% and 20% $H_2S$ cycle ratio) Zn(O,S) films tend to grow more homogeneously, whereas we can discriminate key structural differences in sulfur rich samples (33%). These sulfur rich films are quite distorted when grown on ZnO and thus modify their electronic structure during growth through relaxation events. We discovered the formation of sulfate in Zn(O,S) films and their stronger expression in thin films compared to thick films, showing that these species form at Zn(O,S)/ZnO and Zn(O,S)/$TiO_2$ interfaces. Their formation is independent from film composition and occurs through sulfur's diffusion within the films and into the substrate. This results in degradation of device performance as is already known. Leveraging sulfur's diffusivity, we propose a diffusion enabled alternative ALD deposition method (Diffd) comprising $H_2S$ pulses after full ZnO deposition cycles. Yielding similar results to the conventional laminar method, we challenge future researchers to rethink deposition strategies for oxysulfide ALD films as metal-sulfides might grow in a completely different manner than metal-oxides.

## ■ ASSOCIATED CONTENT

### Supporting Information

The Supporting Information is available free of charge on the ACS Publications website at DOI: 10.1021/acsami.6b04000.

Details on the ALD deposition parameters and experimental measurements, O K-edge of other architectures, as well as atomic force microscopy (AFM) images and an XPS spectrum (PDF)

## ■ AUTHOR INFORMATION


### Corresponding Author

*E-mail: jtorgersen@stanford.edu.


### Notes

The authors declare no competing financial interest.

## ■ ACKNOWLEDGMENTS

The Diversifying Academia Recruiting Excellence of Stanford University funded Dr. Orlando Trejo. Dr. Jan Torgersen was funded by the Austrian Research Fund (FWF) under the contract J3505-N20. The authors would like to thank SNSF for use of PHI VersaProbe Scanning XPS Microprobe for XPS measurements. We also thank the National Accelerator Laboratory (SLAC) for allowing us to gather data using beamlines 4-3 and 10-1 at the Stanford Synchrotron Radiation Lightsource (SSRL). We thank K. Roelofs and S. Bent for materials.

## ■ REFERENCES


(1) Buffière, M.; Harel, S.; Guillot-Deudon, C.; Arzel, L.; Barreau, N.; Kessler, J. *Phys. Status Solidi A* **2015**, *212* (2), 282−290.
(2) Sun, L.; Haight, R.; Sinsermsuksakul, P.; Bok Kim, S.; Park, H. H.; Gordon, R. G. *Appl. Phys. Lett.* **2013**, *103* (18), 181904.
(3) Platzer-Björkman, C.; Lu, J.; Kessler, J.; Stolt, L. *Thin Solid Films* **2003**, *431−432*, 321−325.
(4) Hejin Park, H.; Heasley, R.; Gordon, R. G. *Appl. Phys. Lett.* **2013**, *102* (13), 132110.
(5) Uhm, G.-R.; Jang, S. Y.; Jeon, Y. H.; Yoon, H. K.; Seo, H. *RSC Adv.* **2014**, *4* (53), 28111−28118.
(6) Adel, C.; Fethi, B. M.; Brahim, B. Simulation analysis of the effect graded Zn(O,S) on the performance of the ultra thin copper indium gallium diselenide (CIGS) solar cells. *Int. J. Phys. Sci.* **2014**, *9* (10), 250−254.
(7) Sun, J.; Nalla, V.; Nguyen, M.; Ren, Y.; Chiam, S. Y.; Wang, Y.; Tai, K. F.; Sun, H.; Zheludev, N.; Batabyal, S. K.; Wong, L. H. *Sol. Energy* **2015**, *115*, 396−404.
(8) Meyer, B. K.; Polity, A.; Farangis, B.; He, Y.; Hasselkamp, D.; Krämer, T.; Wang, C. *Appl. Phys. Lett.* **2004**, *85* (21), 4929.
(9) Dadlani, A. L.; Trejo, O.; Acharya, S.; Torgersen, J.; Petousis, I.; Nordlund, D.; Sarangi, R.; Schindler, P.; Prinz, F. B. *J. Mater. Chem. C* **2015**, *3* (47), 12192−12198.
(10) Bakke, J. R.; Tanskanen, J. T.; Hägglund, C.; Pakkanen, T. A.; Bent, S. F. *J. Vac. Sci. Technol., A* **2012**, *30* (1), 01A135.
(11) Platzer-Björkman, C.; Törndahl, T.; Abou-Ras, D.; Malmström, J.; Kessler, J.; Stolt, L. *J. Appl. Phys.* **2006**, *100* (4), 044506.
(12) Thimsen, E.; Baryshev, S. V.; Martinson, A. B. F.; Elam, J. W.; Veryovkin, I. V.; Pellin, M. J. *Chem. Mater.* **2013**, *25* (3), 313−319.
(13) Ramanathan, K.; Mann, J.; Glynn, S.; Christensen, S.; Pankow, J.; Li, J.; Scharf, J.; Mansfield, L.; Contreras, M.; Noufi, R. A comparative study of Zn(O,S) buffer layers and CIGS solar cells fabricated by CBD, ALD, and sputtering. *Photovoltaic Specialists Conference (PVSC), 2012 38th IEEE* **2012**, 1677−1681.
(14) Billinge, S. J. L.; Levin, I. *Science* **2007**, *316* (5824), 561−565.
(15) Trejo, O.; Roelofs, K. E.; Xu, S.; Logar, M.; Sarangi, R.; Nordlund, D.; Dadlani, A. L.; Kravec, R.; Dasgupta, N. P.; Bent, S. F.; Prinz, F. B. *Nano Lett.* **2015**, *15* (12), 7829−7836.
(16) Torgersen, J.; Acharya, S.; Dadlani, A. L.; Petousis, I.; Kim, Y.; Trejo, O.; Nordlund, D.; Prinz, F. B. *J. Phys. Chem. Lett.* **2016**, *7*, 1428−1433.
(17) Dadlani, A. L.; Schindler, P.; Logar, M.; Walch, S. P.; Prinz, F. B. *J. Phys. Chem. C* **2014**, *118* (43), 24827−24832.
(18) Wu, S.; Han, H.; Tai, Q.; Zhang, J.; Chen, B. L.; Xu, S.; Zhou, C.; Yang, Y.; Hu, H.; Zhao, X.-Z. *Appl. Phys. Lett.* **2008**, *92* (12), 122106.
(19) Ramanathan, K.; Contreras, M. A.; Perkins, C. L.; Asher, S.; Hasoon, F. S.; Keane, J.; Young, D.; Romero, M.; Metzger, W.; Noufi, R.; Ward, J.; Duda, A. *Prog. Photovoltaics* **2003**, *11* (4), 225−230.
(20) Ericson, T.; Scragg, J. J.; Hultqvist, A.; Watjen, J. T.; Szaniawski, P.; Torndahl, T.; Platzer-Bjorkman, C. *Photovoltaics, IEEE J.* **2014**, *4* (1), 465−469.
(21) Malm, U.; Malmström, J.; Platzer-Björkman, C.; Stolt, L. *Thin Solid Films* **2005**, *480−481*, 208−212.
(22) Zhang, S.; Du, Y.; Li, H.; Chu, W.; Li, J.; Yan, W.; Wei, S.; Yan, C.; Wu, Z. *J. Phys. Chem. C* **2009**, *113* (11), 4263−4269.
(23) Gilbert, B.; Frazer, B. H.; Zhang, H.; Huang, F.; Banfield, J. F.; Haskel, D.; Lang, J. C.; Srajer, G.; De Stasio, G. *Phys. Rev. B: Condens. Matter Mater. Phys.* **2002**, *66* (24), 245205.
(24) Jalilehvand, F. *Chem. Soc. Rev.* **2006**, *35* (12), 1256−1268.
(25) Heske, C.; Groh, U.; Weinhardt, L.; Fuchs, O.; Holder, B.; Umbach, E.; Bostedt, C.; Terminello, L. J.; Zweigart, S.; Niesen, T. P. *Appl. Phys. Lett.* **2002**, *81*, 4550.
(26) Schmidt, M.; Braunger, D.; Schäffler, R.; Schock, H.; Rau, U. *Thin Solid Films* **2000**, *361−362*, 283−287.
(27) Stuyven, G.; De Visschere, P.; Hikavyy, A.; Neyts, K. *J. Cryst. Growth* **2002**, *234* (4), 690−698.
(28) Tanskanen, J. T.; Bakke, J. R.; Bent, S. F.; Pakkanen, T. A. *Langmuir* **2010**, *26* (14), 11899−11906.




DOI: 10.1021/acsami.6b04000
*ACS Appl. Mater. Interfaces* 2016, 8, 14323−14327